Macromolecular Materials and Engineering
www.mame-journal.de

Evaluation of the Fusion Quality of Bead Foams Made from Polybutylene Terephthalate (E-PBT) Depending on the Processing Temperature

*Justus Kuhnigk, Niko Krebs, Tobias Standau, Marcel Dippold, and Holger Ruckdäschel**

Increasing requirements are leading to new developments in bead foam materials. Engineering thermoplastics such as polybutylene terephthalate (PBT) outperform standard bead foams in thermal stability. In order to obtain molded parts, beads are fused together using steam chest molding. Classical theories for the fusion mechanism, explaining the molding of amorphous EPS (expandable polystyrene) or semi-crystalline EPP (expanded polypropylene), cannot be applied to E-PBT (expanded polybutylene terephthalate). In previous studies, sufficient time for polymer interdiffusion during molding is identified as crucial and requires adjusted crystallization kinetics. This study consequently examines to which extent the crystalline properties and the bead fusion behavior of E-PBT can be influenced by the bead foaming process. By varying the underwater granulation (UWG) water temperature, different cooling rates of the expanding melt are generated. The foamed beads show different cell morphologies, thermal and dynamic mechanical properties depending on the UWG water temperature. Those beads that show a pronounced shrinkage behavior in the thermomechanical analysis, caused by an increased open cell content and a pronounced cold-crystallization, exhibit a reduced bead fusion quality. The bead fusion quality is examined by the fracture surface. The shrinkage phenomenon causes a reduced bead to bead contact and partially separation between the beads.

1. Introduction

Bead foaming has elevated to an established manufacturing route for foams. The bead foaming technology allows both the high foam expansion of extrusion foaming and the geometrical complexity of the resulting part of the injection molding process. The two-step manufacturing process consists of (i) foaming and (ii) fusing micro cellular single beads into molded parts.[1–5] In the history of bead foams the first 50 years only focussed on the commodity plastics polystyrene (as expandable polystyrene (EPS)[6,7]), polyethylene (as expanded polyethylene (EPE)[8,9]), and polypropylene (as expanded polypropylene (EPP)[10–12]). These materials are cost-efficient applications that require good insulating properties and high energy absorption.[13] However, this small group of polymers limits application. One drawback of the previous mentioned matrix polymers is the low long-term heat resistance temperature (i.e., 80 °C for EPS and 110 °C for EPP,[14,15] respectively) which hinders certain applications (e.g., close to the engine, so-called under-the-hood applications) and processes (e.g., cathodic dip painting and subsequent IR drying). First bead foams for elevated temperature applications are described in literature or are already commercially available, i.e., PMI (polymethacrylimide) (Evonik AG),[16] PET (polyethylene terephthalate) (Armacell S.A.),[17] PA (polyamide) (BASF SE, Asahi Kasei K.K.),[18–21] PC (polycarbonate) (Covestro AG),[22] and PESU (polyethersulfone) (BASF SE).[23] Another example is expanded polybutylene terephthalate (E-PBT) manufactured in a continuous bead foam extrusion process.[24]

To produce parts, individual beads are typically molded by hot steam, which is well explained in the literature for EPS, EPE, and EPP.[1] Previous investigations by Standau et al.[25,26] showed that unmodified PBT bead foams cannot be fused into a molded part, while fusability can be achieved by chemical modification with a multifunctional epoxy based chain extender (CE). The bead fusion mechanism of E-PBT differs significantly from established amorphous and semicrystalline polymers (EPS and EPP). As an amorphous polymer, EPS has a wide softening range, so the energy introduced in the molding process as steam causes the indi-

J. Kuhnigk, N. Krebs, T. Standau, M. Dippold, H. Ruckdäschel
Department of Polymer Engineering
University of Bayreuth
95447 Bayreuth, Germany
E-mail: holger.ruckdaeschel@uni-bayreuth.de
H. Ruckdäschel
Bavarian Polymer Institute and Bayreuth Institute of Macromolecular Research
University of Bayreuth
95447 Bayreuth, Germany

The ORCID identification number(s) for the author(s) of this article can be found under https://doi.org/10.1002/mame.202200419

DOI: 10.1002/mame.202200419

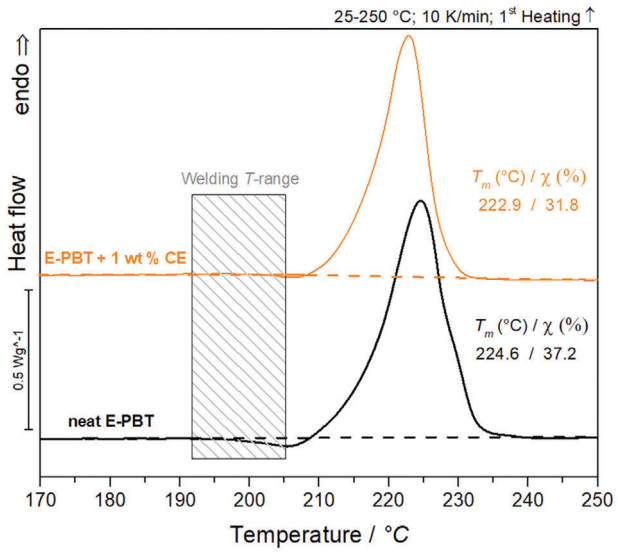

Figure 1. DSC analysis of neat and 1 wt% CE modified E-PBT.[34]

vidual beads to be heated above T_g. As a result, the chain mobility is increased and consequently, the chains can interfuse and entangle across the bead borders. At the same time the mechanical stiffness is still high enough to ensure sufficient dimensional stability of the entire foam structure.[27–33] EPP is a semi-crystalline bead foam produced in stirring autoclave process. An isothermal saturation step in the autoclave at elevated temperature leads to the formation of a high-temperature melting peak with a more perfect crystal structure. During cooling the low melting peak is formed. This procedure results in a characteristic double melting peak, which is essential for the sintering of the beads. During molding the steam temperature exceeds the first peak; yet, the molten crystals of the low melting peak enable welding. Though, the high-temperature peak is not exceeded and represents the higher-order crystalline regions that are responsible for the dimensional stability of the foam structure during sintering. Classical theories explaining the moldability of EPP fail to describe E-PBT as no double melting peak could be detected. E-PBT shows only one melting peak and fuses well below the melting temperature. Moreover, E-PBT can only be molded sufficiently when chain extender (CE) was added. In previous investigations we were able to gain more insights into the bead fusion mechanism of E-PBT.[34,35] In the temperature range where the molding process takes place (**Figure 1**), unmodified E-PBT crystallizes faster than CE modified E-PBT as indicated by a cold-crystallization peak. We could show that the incorporation of chain extender significantly increases the steric hindrance, slows down crystallization and reduces cold-crystallization in the fusion temperature range. Consequently, the time available for interdiffusion of chains across neighboring beads increases and facilitates crystallization across the inter-bead interface. Therefore, it was concluded that sufficient time for polymer interdiffusion during molding is crucial and requires adjusted crystallization kinetics.

The present study builds on this conclusion and addresses the central question of how the crystallization behavior and consequently the bead fusion behavior of PBT can be influenced by the bead foaming process. During this process the blowing agent

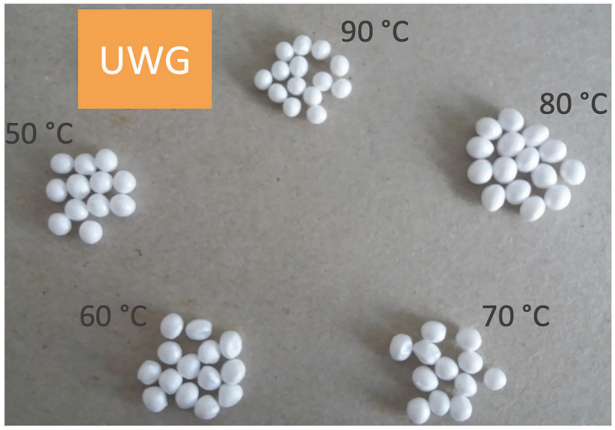

Figure 2. Optical appearance of the produced bead foams, at different UWG water temperatures.

loaded melt strand is extruded at high pressure through a die plate with circular holes into a water stream where it expands due to the pressure drop and where it gets permanently cut by a fast rotating knife. The foamed beads are formed. The water temperature can be varied, which has potentially influence on the expandability (i.e., density and cell morphology) and the surface properties (e.g., crystallinity and roughness) of the beads. For this reason, the water temperature of the underwater granulator (UWG) was varied and its influence on the thermal properties and the bead fusion potential of the resulting beads was investigated. The fusion quality can be judged by the fracture pattern of broken samples. Here, the failure can appear (i) between the beads (surfaces) leaving the beads itself unaffected (so called inter-bead fracture) and/or (ii) within the beads (so called intra-bead-fracture). This was done by Rossacci et al.,[30] who determined the fusion quality of EPS molded parts from the ratio of inter- and intra-bead failure under tensile load by analyzing the structure of broken specimens. In order to ensure comparability of the materials and to work out the influence of the process only one material formulation (PBT + 1 wt% CE @ 2 wt% CO_2) was selected in this study.

2. Results and Discussion

2.1. Optical Appearance and Cell Morphology

The process is stable at UWG water temperatures from 50 to 80 °C. However, the process becomes unstable at a UWG water temperature of 90 °C so that only a few beads could be produced. The reason for this unstable process control is likely based on the fact that the 90 °C hot water can easily boil when it comes into contact with the hot expanding polymer melt. **Figure 2** shows a picture of the produced bead foams. No visual differences between the individual bead types can be seen. Neither the shape nor the size and coloring are significantly influenced by a change of the UWG water temperature between 50 °C and 80 °C. However, the beads at 90 °C are clearly smaller, which is also reflected by a significantly higher density.

The densities and cell densities of the bead foams are plotted in **Figure 3** as function of the UWG water temperature. The SEM

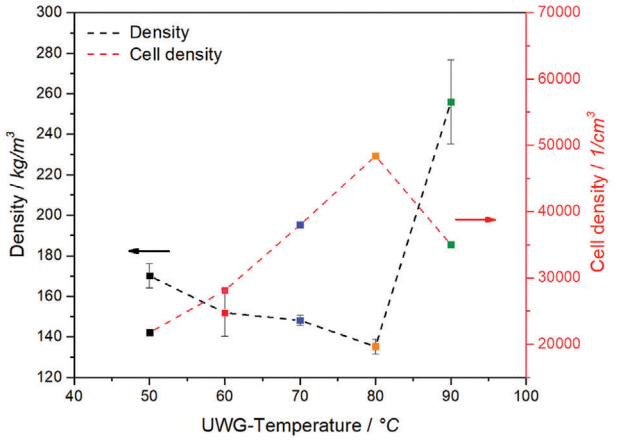

Figure 3. Plot of the bead foam density and cell density as a function of the UWG temperature.

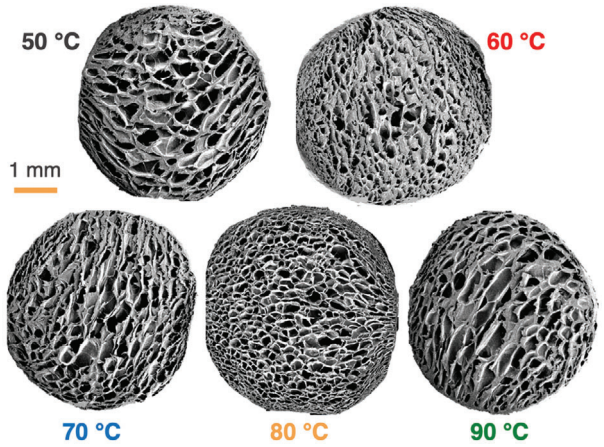

Figure 4. Morphologies of CE modified PBT beads obtained at different UWG water temperatures varying from 50 to 90 °C.

images of the cell morphologies of the bead foams in Figure 2 were used to evaluate the cell densities.

The lowest density is achieved at 80 °C (135 ± 4 kg m^{-3}). With decreasing temperature, a slight increase in density can be seen (50 °C; (170 ± 6 kg m^{-3}), 60 °C (152 ± 11 kg m^{-3}), and 70 °C (148 ± 3 kg m^{-3})). At 90 °C a large density increase (256 ± 21 kg m^{-3}) is observed. During the underwater pelletizing process, the hot expanding melt comes into contact with the much colder water of the UWG unit. The cooling rate is lower at higher UWG water temperatures. Subsequently, the polymer inside the beads stays longer in a viscosity range that allows cell growth. The resistance to expansion is greater at lower temperatures and prevents further expansion of the blowing agent. Up to an UWG water temperature of 80 °C, the density decreases accordingly. At an UWG water temperature of 90 °C, the viscosity is lower, so that effects such as cell coalescence and cell collapse occur more frequently. This phenomenon is also supported by the morphology (**Figure 4**). In addition, the optimum cell density is visible at an UWG water temperature of 80 °C (48 400 cells cm^{-3}). The cell density increases continuously from 50 to 80 °C. The cell density at 90 °C (35 000 cells cm^{-3}) is outside the trend. The

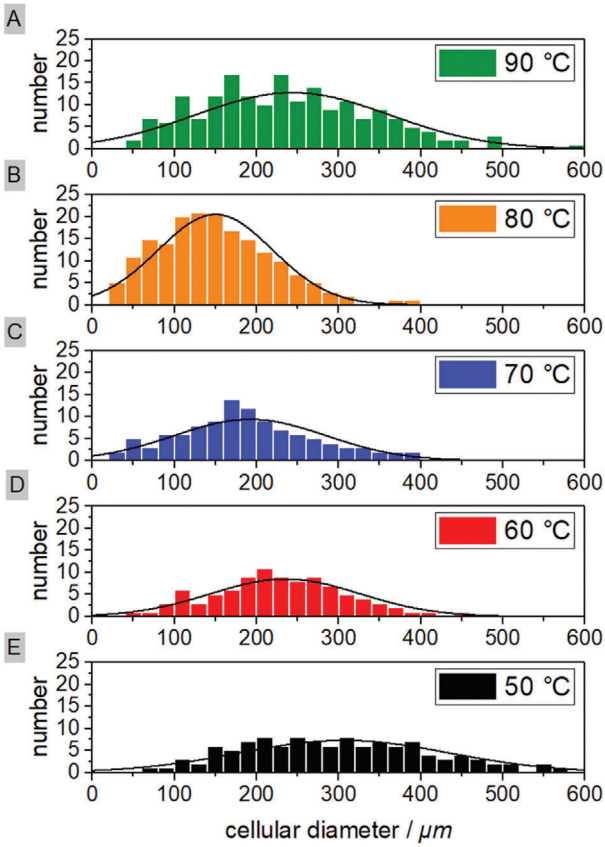

Figure 5. Cell size distributions at different UWG water temperatures.

number of cells depends strongly on the number of nucleation nuclei and their growth rate. The number of nuclei is greater at a lower temperature (increasing supercooling → thermodynamic driving force), but the nucleation growth rate also decreases very quickly, so that fewer of the nuclei formed reach the critical nucleus size and can thus form a cell.[36] At higher temperatures or lower cooling rates, the necessary energy barrier for reaching the critical nucleus size is reached. Therefore, at higher UWG water temperatures, more cells are formed, which cause the higher cell density. At a water temperature of 90 °C, the core of the bead cools down the slowest compared with the beads produced with lower UWG water temperatures. The core of the bead remains at higher temperatures and the viscosity stays lower. Yet, the polymer chains remain with higher mobility for a longer time and the formed cells can grow for a longer time, which causes cell collapse and cell coalescence.

The beads processed at a UWG water temperature of 50 °C show some large elongated cells, whereas clearly more smaller and round cells are observed at a UWG water temperature of 80 °C. The foamed beads at 90 °C show many elongated cells as a result of the cell coalescence. For a more precise assessment, the cell size distributions at the respective UWG water temperatures are shown as histograms (**Figure 5**). The distributions (trend line calculated according to Gaussian normal distribution) become narrower with increasing UWG water temperature up to 80 °C. The most stable cell growth, as related to a homogeneous cell size distribution, takes place at 80 °C UWG water temperature.

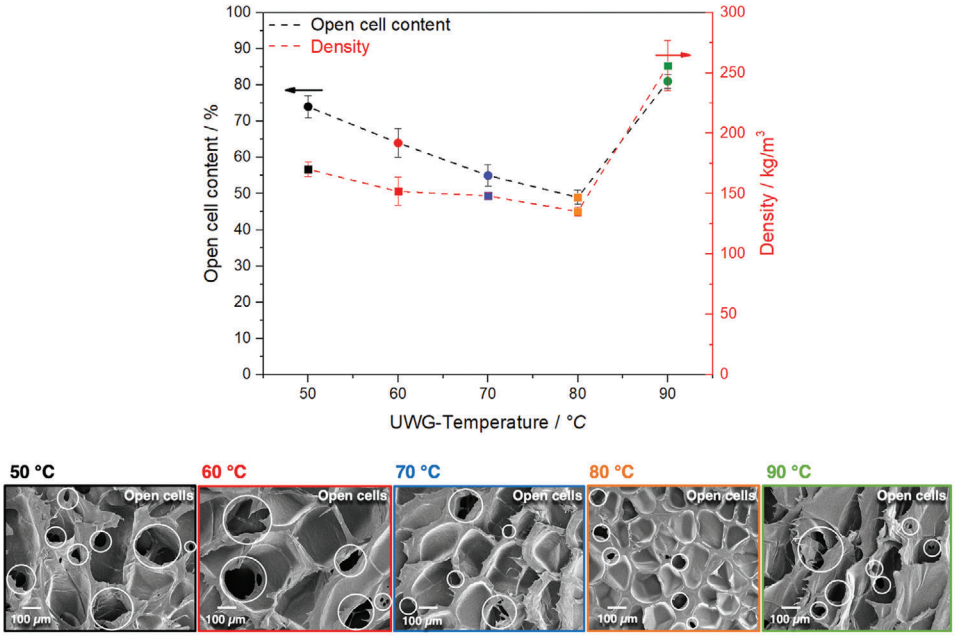

Figure 6. Open cell content as function of the UWG water temperature (top) and SEM micrographs of the foamed beads (bottom).

From a thermodynamic point of view, cell growth is favored with increasing temperature. The fact that the cell sizes are nevertheless smaller with increasing UWG water temperature is due to the growth site impingement, crowding and truncation of several growing cells, compared to lower UWG temperatures.[37] As already mentioned, the reduced viscosity level at 90 °C favors phenomena such as cell coalescence and cell collapse, so that the cell size distribution also becomes broader again.

2.1.1. Open Cell Content (OCC)

In order to investigate the impact of UWG water temperature on the stability of the nucleated cells, the OCC of the PBT foam beads was measured. **Figure 6** shows that bead foam density and OCC follow the same trend as function of the UWG water temperature. The OCC decreases with bead density. This correlation is already well known in literature.[38] As soon as the cell wall ruptures, the cell gas escapes rapidly, resulting in a significant gas loss, which prevents the cell from further growth and leads to less expansion (i.e., comparably higher density). The fact that the OCC increases at lower UWG water temperatures is due to the lower rate of gas loss (gas diffusivity), which potentially contributes to expansion.[39] This phenomenon is most pronounced at an UWG water temperature of 50 °C (below T_g of PBT), so that an overexpansion is caused and cell fractures occur more frequently. In addition, at a UWG water temperature of 50 °C PBT is below the glass transition temperature, so that internal stresses can't be relieved easily. Above the glass transition temperature, there is a higher chain mobility so that the internal stresses can be relieved by deformation. Up to an UWG water temperature of 80 °C, the material becomes more flowable and the OCC decreases accordingly. At an UWG water temperature of 90 °C, the melt strength of the expanding melt is so low, that effects such as cell coalescence and cell collapse occur more frequently and the OCC is high.

2.1.2. Thermal Characterization (DSC)

Crystallization effects on the bead surface are expected to play a crucial role for the bead fusion process of E-PBT.[34,40] For this reason, the crystallization behavior of the bead foams is considered separately here. The thermal history, which is determined by the process, plays an important role. Therefore, especially the first heating curves of the DSC thermograms are considered. Crystalline properties of the outer layers are considered since the formation of inter-bead bonding involves the diffusion of the amorphous compartments of the polymer chains and cross crystallization across the interfaces. From these measurements, important information is obtained about the total crystallinity, which reflects the initial situation before the steam chest molding process (i.e., fusion), and the cold-crystallization, i.e., the ability to continue crystal growth below the melting point during the bead fusion process. **Figure 7** shows the first heating curves of outer layer of beads processed at different UWG water temperatures.

The melting points T_m of the individual samples are similar and no trend is discernible. The crystallinity χ slightly decreases with decreasing UWG water temperature. These observations can be attributed to two phenomena. With increasing UWG water temperature, the density in the bead decreases. The higher expansion rates are accompanied by a greater orientation of polymer chains, i.e., the proportion of strain-induced crystallization increases. Furthermore, in previous studies[34] we already showed that the extent of crystallinity decreases with increasing cooling rate. The UWG water temperature has no influence on the glass transition temperature (about 58 °C for all samples). This has a direct influence on crystallization, because below the glass

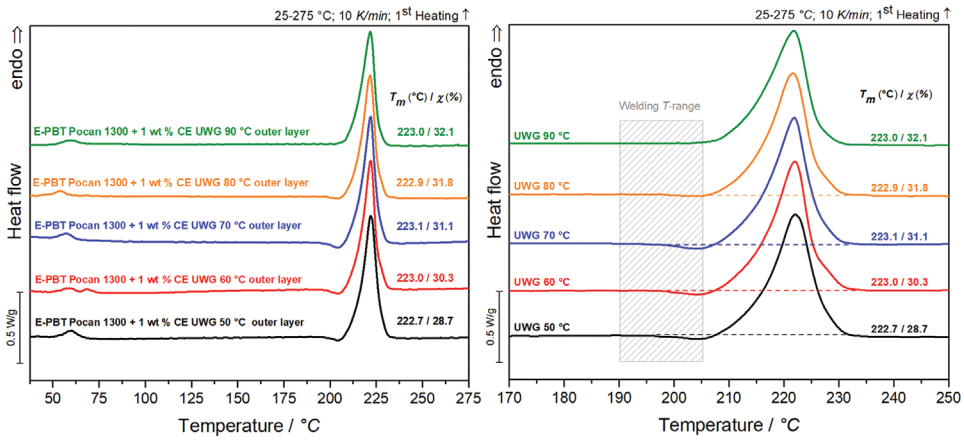

Figure 7. DSC thermogram of the first heating curve of the obtained bead foams obtained at different UWG water temperatures.

Table 1. Summary of the thermal data determined by the DSC measurements.

UWG water temperature [°C]	Crystallinity χ [%]	Enthalpy of fusion ΔH_m [J g^{-1}]	Melting point T_m [°C]
50	28.7	40.1	222.7
60	30.3	42.4	223.0
70	31.1	43.5	223.1
80	31.8	44.5	222.9
90	32.1	44.9	223.0

transition temperature the freedom of movement is too low to crystallize further. Due to the faster cooling of the polymer at lower UWG water temperatures, the existing state is frozen more quickly. With decreasing UWG water temperature, the mobility of the chains decreases, so that crystal growth is also impaired. The fact that the crystallization process in the UWG is not complete is reflected in the appearance of a cold-crystallization peak in the first heating curve. The lower the UWG water temperature or the less time the system was given to crystallize during the UWG process, the more pronounced this peak appears in the first heating curve. It is worth to mention that the cold-crystallization peaks occur in the temperature range of bead fusion. All relevant values of the DSC measurement are summarized in **Table 1**.

2.1.3. Thermomechanical (TMA) and Dynamic Mechanical Thermal Analysis (DMTA)

Expansion with increasing temperature and contraction during cooling are reversible mechanisms of polymer materials. In addition, polymers with frozen-in stresses show irreversible stress relaxation when the sample is heated up.[41] During the bead foam process, the internal CO_2 gas pressure of the foam cells causes an equibiaxial expansion of the surrounding melt. Through the underwater pelletizing process the oriented and stretched polymer chains are frozen in that state by rapidly cooling in water. The polymer chains do not have enough time to relax and remain frozen in a tensed way. Using the TMA method (**Figure 8**), foamed beads produced at different UWG water temperatures show both effects, reversible thermal expansion and irreversible stress relaxation (shrinkage). During the bead fusion process, hot steam is introduced into a cavity in which the bead foams are compressed due to the back pressure. The beads are heated from room temperature to the fusion temperature via steam and then sintered at a constant temperature. The heating behavior of the beads in the cavity is simulated using TMA in order to get more insights into bead fusion mechanism of E-PBT.

Below the glass transition temperature (T_g around 58 °C according to Figure 7), all foamed beads produced at different UWG water temperatures show only slight volume expansion (ideal linear thermal expansion) with increasing temperature due to their low chain mobility. When exceeding the T_g the beads change from a structural configuration of limited or no chain mobility to an increased chain mobility state and revert to their more entangled configuration. Driving force is the reduction of frozen tension which results in a volume shrinkage of the beads. This stress relaxation phenomenon is more pronounced the more the expanded beads were cooled in the UWG process. At a UWG water temperature of 50 °C (below T_g), the beads are most strongly quenched and stress relaxation is most pronounced accordingly. At a UWG water temperature of 80 and 90 °C (above T_g), the polymer chains possessed a higher chain mobility, so that a large part of the internal stresses could already be relieved during the process and therefore hardly any relaxation behavior is visible in the TMA diagram. The volume shrinkage is associated with a densification, which is expressed in a stiffness change of the material. In the DMTA diagram (**Figure 9**), the bead stiffness decreases in the temperature range between 75 and 100 °C with different slopes, for the beads processed at an UWG water temperature of 50 °C the slowest, due to the relaxation-induced volume shrinkage and the associated densification. For all curves considered, shrinkage is followed by expansion. On the one hand caused by the typical thermal expansion of PBT, on the other hand the gas stored in closed cell expands with increasing temperature and causes a volume expansion of the closed cells. With decreasing OCC (Figure 6), a stronger volume expansion is caused. In addition, the cell gas causes a plasticizing effect which reduces the bead stiffness and the material becomes softer, so that the cells are less resistant to stretching. Accordingly, the volume expansion is most pronounced for beads produced at a UWG water temperature of

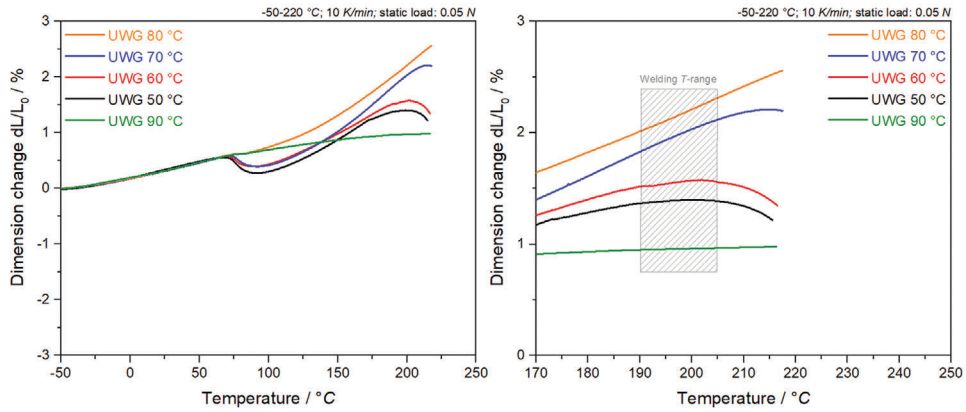

Figure 8. TMA single bead measurements of bead foams processed at different T_{UWG}.

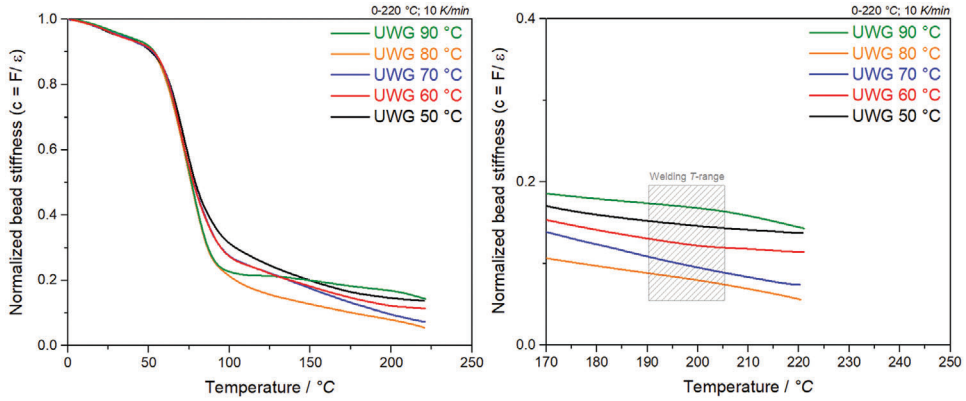

Figure 9. DMTA single bead measurements of bead foams processed at different T_{UWG}.

80 °C (lowest OCC) and most weakly pronounced for beads produced at 90 °C (highest OCC).

In the temperature range around 200 °C, the volumetric shrinkage results from the densification upon cold-crystallization (chain folding). This also manifests itself in a less rapidly decreasing bead stiffness in this temperature range. Cold-crystallization is most pronounced at an UWG water temperature of 50 °C and least pronounced at 80 and 90 °C, and the extent of shrinkage and the slope behavior of the bead stiffness behave accordingly (Figure 7).

During molding, chain inter-diffusion across the bead interfaces occurs in a thin layer on the surfaces of two touching foamed beads resulting in a strong physical bond. Therefore, a large contact area between the beads is a prerequisite for optimal bead fusion. Regarding the TMA measurement, beads that show volume expansion instead of shrinkage during the steam chest molding process are expected to be more suitable. Entanglements of the chains of neighboring beads across the interfaces also requires a certain chain mobility in the temperature range in which the fusion occurs. The higher the chain mobility, the better the bead fusion process should be. If the stiffness of the bead decreases, while retaining the dimension, the beads can nestle together better and form a larger contact area, which is advantageous for the interdiffusion process.

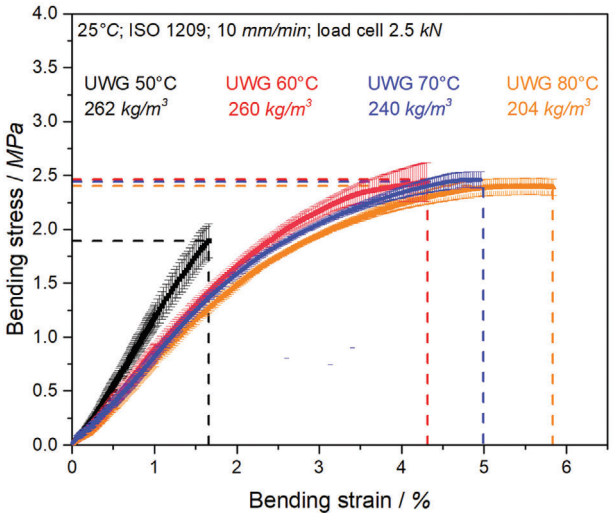

Figure 10. Plot of bending stress against bending strain by a three-point bending test.

Table 2. Summary of the mechanical characteristic values as a function of the UWG temperature.

UWG water temperature [°C]	Density [kg m^{-3}]	Bending modulus [MPa]	Bending strength [MPa]	Deformation at break [%]
50	262 ± 3	117 ± 13	1.85 ± 0.20	1.6 ± 0.1
60	260 ± 2	94 ± 21	2.45 ± 0.37	4.4 ± 0.4
70	240 ± 3	89 ± 14	2.44 ± 0.19	5.0 ± 0.6
80	204 ± 1	81 ± 10	2.40 ± 0.22	5.8 ± 0.7

2.1.4. Welding of the Beads

Molded parts were produced from the beads processed at different UWG water temperatures. It was not possible to produce a molded part from the foamed beads processed at 90 °C because the unstable process did not provide sufficient yield of foamed beads. The density of the molded parts obtained varied. The E-PBT plate processed at a water temperature of 80 °C shows the lowest density of 204 kg m^{-3} (density of the other plates: 70 °C: 240 kg m^{-3}; 60 °C: 260 kg m^{-3}; 50 °C: 262 kg m^{-3}). For a precise evaluation of the bead fusion quality, all molded parts were tested by three-point bending and the fracture surfaces were analyzed by SEM images. **Figure 10** shows the mechanical characterization of the molded part by three-point bending tests. **Table 2** lists the mechanical parameters of the individual samples.

The mechanical values of a foam are strongly dependent on its density. The densities of the molded parts for UWG water temperatures of 50 and 60 °C are almost identical allowing a direct comparison of the mechanical values. While the bending modulus decreases slightly, the fracture stress at break and the deformation at break increase. Increasing UWG water temperature ultimately results in molded parts with lower densities. Even though the densities vary between the different molded parts, trends in the mechanical properties can be derived. As the UWG water temperature rises, the bending modulus in the corresponding molded part decreases slightly. The deformation at break increases significantly with increasing UWG water temperature, the fracture stress also increases from 50 to 60 °C and shows for 60, 70, and 80 °C more or less the same fracture stress.

The fracture patterns shown in **Figure 11** can be used for a more detailed interpretation of the mechanical behavior. The intra-bead failure continuously increases with UWG water temperature (Figure 11A–D). The intra-bead failure is a quality feature of interdiffusion and its bonding effect, because here the surfaces are stronger connected than the cells within a bead. Based on the areas of the respective failure type, the corresponding proportion of inter-bead and intra-bead failure can be determined. The intra-bead content in the component increases for beads processed at higher UWG water temperatures, consequently component failure also occurs at higher bending strains. Explanations for the different interdiffusion potentials of the beads can be related to the previous findings of the individual beads (DSC, TMA, DMTA). Those beads that show a pronounced shrinkage behavior in the thermomechanical analysis, caused by an increased OCC (Figures 6 and 8) and a pronounced cold-crystallization (Figure 7), exhibit a reduced bead fusion quality. The shrinkage phenomenon causes an increased distance between the beads in the cavity and thus increases the diffusion paths between the bead interfaces. It is also evident that cold-crystallization occurs in the welding temperature range. The result is not only a volume shrinkage, but also an increase in storage modulus due to the

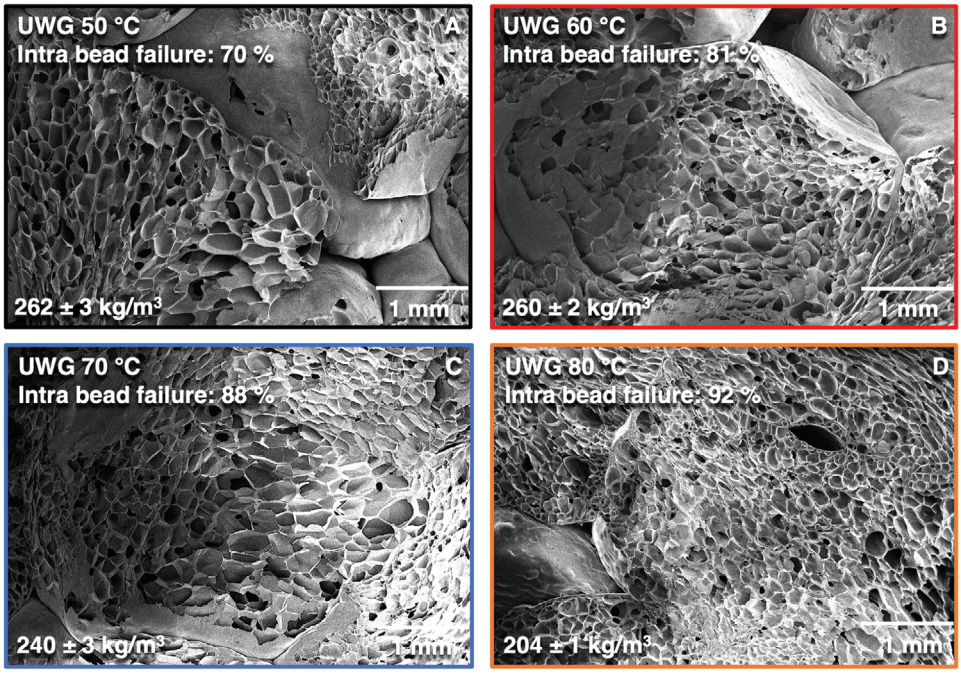

Figure 11. Fracture surfaces observed by SEM of different molded foam parts made of bead foams processed at different UWG water temperatures of A) 50 °C, B) 60 °C, C) 70 °C, and D) 80 °C.

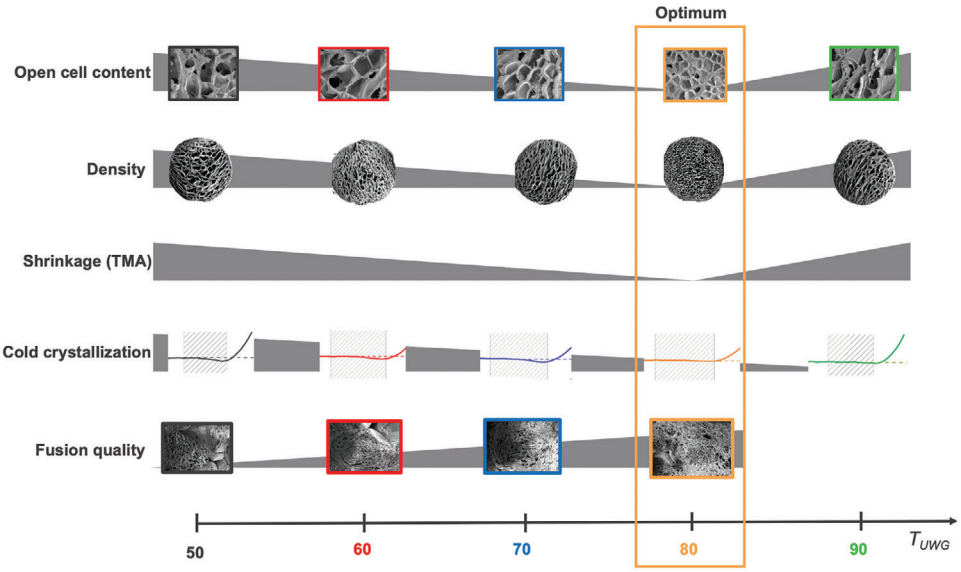

Figure 12. Overview diagram of the parameters that influence molding of the beads processed at different UWG water temperatures.

conditional densification (Figure 9), which decreases the chain mobility and consequently the entanglement ability between the bead interfaces.

3. Conclusions

For E-PBT bead foams sufficient time for polymer interdiffusion during molding is crucial and requires adjusted crystallization kinetics. During the under-water granulation (UWG), the expanding PBT melt comes in contact with the much colder water. In our study, different cooling rates have been generated by varying the UWG water temperature during the bead manufacturing process. Their impact on the cell morphology, thermal and dynamic mechanical properties has been examined. Technically temperatures above the boiling point of water (100 °C) should not be exceeded. We experienced that process fluctuations can appear at 90 °C. However, at 80 °C the process runs stable. From a scientific point of view we could show a clear trend with increasing water temperature; we see the identification of a possible optimum between 80 and 90 °C as technical fine tuning.

Subsequently, correlations to the fusion quality of the corresponding molded parts were developed (**Figure 12**). The lower the UWG water temperature (e.g., UWG 50 °C) or the less time the system was given to crystallize (UWG 50 °C: crystallinity of 28.7%) during the UWG process, the more pronounced is the appearance of a cold-crystallization peak in the first heating curve in the DSC. In addition, the beads cooled at lower UWG water temperatures (e.g., UWG 50 °C) show increased shrinkage behavior in TMA measurements due to their frozen-in stresses and their increased OCC (UWG 50 °C: OCC of 74%). Furthermore, the volume shrinkage phenomenon causes an increase in the bead stiffness due to the conditional densification, which decreases the chain mobility and consequently the entanglement ability between the bead interfaces. Accordingly, those beads that show a pronounced shrinkage behavior in the thermomechanical analysis, caused by an increased OCC and a pronounced cold-crystallization, exhibit a reduced bead fusion quality as verified by a lower intra-bead failure (UWG 50 °C: intra bead failure of 70%) content.

4. Experimental Section

Materials: PBT Pocan B1300 was kindly provided by Lanxess AG (Cologne, Germany). Prior to processing the material was dried at 80 C for 4 h. For chemical modification, the multifunctional epoxy chain extender Joncryl ADR 4468 from BASF SE (Ludwigshafen, Germany) was used.

Processing: The production of the foamed beads by using a Dr. Collin tandem foam extrusion line (Ebersberg, Germany) coupled with an underwater granulator LPU from Gala Kunststoff- und Kautschukmaschinen GmbH (Xanten, Germany) was described in our previous works[25] (A-Extruder: screw speed of 150 rpm, zone 1 to 8: 25/165/190/215/235/245/245/245 °C, B-Extruder: screw speed of 15 rpm, zone 1 to 4: 220/220/220/220 °C). At a throughput of 8 kg h^{-1}, PBT was chemically modified with 1 wt% CE and foamed with 2 wt% CO_2. The water temperature of the UWG was varied in a range of 50 to 90 °C.

To fuse the foamed beads, a steam chest molding machine Teubert TVZ 162/100PP (Blumberg, Germany) was used. This device is equipped with a specialized steam generator HaeCo II from Unibell (Hwaseong, South Korea) which is able to provide high steam pressures of up to 25 bar. The pressures for molding are 13–15 bar. Molding times were 30–45 s. The resulting parts had a dimension of 200 × 300 × 20 mm^3.

Analyses of Foam Morphology and Density: Scanning electron microscopy (SEM) images were taken with a JEOL JSM-6510 (Borken, Germany) at 1.5 kV. Using ImageJ as software, cell sizes were statistically calculated as an average of all cells of the whole cross section of a bead. Three beads per sample were analyzed; i.e., over 100 cells were considered.

The foam density was determined with the Archimedes principle using a Mettler Toledo AG245 balance (Columbus, OH, USA) with density a kit.

Open Cell Content (OCC): The OCC of the E-PBT bead foams was determined using a gas pycnometer (Ultrafoam 1000 Model UPY-15F, Quantochrome Instruments, Boynton Beach, FL, USA) according to ASTM D-6226. A cell with a volume of 10 cm^3 was used for the measurement and the foam samples were exposed to 0.6 bar nitrogen. Three samples of each E-PBT type were measured and three runs were performed for each sample.

Thermal Characterization: The thermal behavior of the E-PBT beads was determined by differential scanning calorimetry (DSC 1) from Mettler Toledo (Columbus, OH, USA). The samples (between 5 and 8 mg) were heated in nitrogen atmosphere in a temperature range from 25 to 275 °C at a heating rate of 10 K min^{-1}. The degree of crystallinity was determined from the ratio of heat of fusion to the theoretical value for the heat of fusion of 100% crystal PBT (140 J g^{-1}) from literature.[42] The evaluation was carried out with the STARe-software (Mettler-Toledo AG, Schwerzenbach, Switzerland) according to Khanna et al.[43] with a straight base line.

Mechanical Testing: Thermomechanical analysis (TMA) of the samples was performed on a TMA Q400 EM from TA Instruments (New Castle, Delaware). The single E-PBT beads (average diameter of 5 mm) were placed under the expansion tool. The expansion curves result from loading the beads under compression force of 0.05 N. The samples were heated up to a temperature of 220 °C with a heating rate of 10 K min^{-1}.

Dynamic Mechanical Thermal Analysis (DMTA): DMTA was performed on a Gabo Eplexor 500 N (Ahlden, Germany) in compression mode on single E-PBT beads (average diameter of 5 mm) by a dynamical oscillating force (0.5 N, preload of 1.0 N) at a frequency of 1 Hz with simultaneous heating up to 220 °C at a heating rate of 10 K min^{-1}. No modulus was determined in the evaluation, since a constant unit area on which a force acts is used for the calculation, which is not the case with a round bead geometry. Instead, the bead stiffness was determined, which is calculated from the acting force and the resulting strain.

Three-point bending experiments were carried out according to ISO 1209 with a universal testing machine 1475 from Zwick Roell (Ulm, Germany), with a testing speed of 10 mm min^{-1} and a 2.5 kN load cell. The molded E-PBT parts with dimensions of 120 × 25 × 20 mm^3 were skinned by grinding off the outer layers to suppress the influence.

Acknowledgements

The authors would like to thank the Deutsche Forschungsgemeinschaft (DFG) for funding this project (AL-474/42-1). They also acknowledge all students, technicians, and scientific members who were involved in the trials and thank them for their support and fruitful discussion. Special thanks to Ute Kuhn for TMA and DMA measurements, Sebastian Gröschel for carrying out the extrusion trials, Annika Pfaffenberger for SEM measurements and to Max Löhner from Neue Materialien Bayreuth GmbH for steam chest molding.

Open access funding enabled and organized by Projekt DEAL.

Conflict of Interest

The authors declare no conflict of interest.

Data Availability Statement

The data that support the findings of this study are available from the corresponding author upon reasonable request.

Keywords

bead foam, bead fusion, bending test, chemical modification, polybutylene terephthalate

Received: June 22, 2022
Revised: July 27, 2022
Published online: August 15, 2022

[1] D. Raps, N. Hossieny, C. B. Park, V. Altstädt, *Polymer* **2015**, *56*, 5.
[2] J. Kuhnigk, T. Standau, D. Dörr, C. Brütting, V. Altstädt, H. Ruckdäschel, *J. Cell. Plast.* **2022**, *58*, 707.
[3] D. Eaves, *Handbook of Polymer Foams*, Rapra Technology, Shrewsbury, UK **2004**.
[4] R. Britton, *Update on Mouldable Particle Foam Technology*, Rapra Technology, Shrewsbury, UK **2009**.
[5] S. T. Lee, *Polymeric Foams*, Taylor and Francis Group, Boca Raton **2022**. ISBN 9781003166160.
[6] F. Stastny, R. Gaeth, Process for the production of porous masses from polymers DE 845264C **1952**.
[7] J. Noordegraaf, F. P. A. Kuijstermann, J. P. M. De Jong, U.S. Patent Application No. 13/122, 960, 14 April **2011**.
[8] L. C. Rubens, W. E. Alexander, U.S. Patent Application US4108934A **1978**.
[9] M. A. Spalding, A. Chatterjee, *Handbook of Industrial Polyethylene and Technology: Definitive Guide to Manufacturing, Properties, Processing, Applications and Markets Set*, Wiley-VCH, Weinheim **2017**.
[10] PlasticsEurope, EPRO, Plastics—the Facts 2016. An analysis of European plastics production, demand and waste data, *Plast.—Facts 2016*. **2016**. Accessible under www.plasticseurope.de/informations.
[11] M. Nofar, Y. Guo, C. B. Park, *Ind. Eng. Chem. Res.* **2013**, *52*, 2297.
[12] N. Hossieny, A. Ameli, C. B. Park, *Ind. Eng. Chem. Res.* **2013**, *52*, 8236.
[13] C. Trassl, V. Altstädt, *Kunstst. Int.* **2014**, *2*, 73.
[14] S. E. BASF, P. Neopolen, Designed for new ideas **2012**.
[15] BASF Aktiengesellschaft, Styropor-technical information **1992**, pp. 1–7.
[16] T. Richter, S. Schwarz-Barac, K. Bernhard, I. Liebl, M. Schnabel, S. Schweitzer, D. Poppe, J. Vorholz, U.S. Patent Application US20150361236A1 **2015**.
[17] J. P. Strasser, WO2011063806A1 **2011**.
[18] O. Kriha, K. Hahn, P. Desbois, V. Warzelhan, H. Ruckdäschel, M. Hofmann, C. Exner, R. Hingmann, Expandable Polyamide Granules WO2011/134996A1 **2011**.
[19] M. Kondo, Y. Fujino, U.S. Patent Application US10167373B2 **2019**.
[20] Press Release, BASF SE, BASF develops Ultramid particle foam for a wide range of applications **2019**. Available online: https://www.basf.com/global/en/products/plastics-rubber/fairs/k-fair-2019/press-room/basf-develops-ultramid–particle-foam-for-a-wide-range-of-applic.html) (Accessed: February 2022).
[21] D. Dörr, D. Raps, D. Kirupanantham, C. Holmes, V. Altstädt, *AIP Conf. Proc.* **2020**, *2205*, 020037. https://doi.org/10.1063/1.5142952.
[22] N. Weingart, D. Raps, J. Kuhnigk, A. Klein, V. Altstädt, *Polymers* **2020**, *12*, 2314.
[23] K. Hahn, M. Hofmann, H. Ruckdäschel, J. K. W. Sandler, Scherzer, Particle Foam Based on a Polymer including Polystyrene, Styrene Copolymer, Polysulfone or Polyethersulfone, Comprises Inorganic Filler, e.g., Talc Having Specified Particle Size and Wax or Oligomer Based Nucleating Agent, e.g., Polyethylene: Partikelschaumstoffe mit verbesserter Steifigkeit DE102011110216A1 **2011**.
[24] T. Köppl, D. Raps, V. Altstädt, *J. Cell. Plast.* **2014**, *50*, 475.
[25] T. Standau, B. Hädelt, P. Schreier, V. Altstädt, *Ind. Eng. Chem. Res.* **2018**, *57*, 17170.
[26] T. Standau, K. Hilgert, J. Kuhnigk, V. Altstädt, H. Ruckdäschel, Influence of Processing Conditions on the Appearance of Bead Foams Made of the Engineering Thermoplastic Polybutylene Terephthalate (E-PBT). SPE Foam 13–16 Sept **2021** Virtual Conf.
[27] R. P. Wool, B.-L. Yuan, O. J. McGarel, *Polym. Eng. Sci.* **1989**, *29*, 1340.
[28] Y. H. Kim, R. P. Wool, *Macromolecules* **1983**, *16*, 1115.
[29] H. Qiu, M. Bousmina, *Macromolecules* **2000**, *33*, 6588.
[30] J. Rossacci, S. Shivkumar, *J. Mater. Sci.* **2003**, *38*, 2321.
[31] H. G. Yuan, G. Kalfas, W. H. Ray, *J. Macromol. Sci., Part C* **1991**, *31*, 215.
[32] P. R. Stupak, W. O. Frye, J. A. Donovan, *J. Cell. Plast.* **1991**, *27*, 484.

[33] D. J. Fossey, C. H. Smith, K. B. Wischmann, *J. Cell. Plast.* **1977**, *13*, 347.
[34] J. Kuhnigk, D. Raps, T. Standau, M. Luik, V. Altstädt, H. Ruckdäschel, *Polymers* **2021**, *13*, 582.
[35] C. Mielke, J. Kuhnigk, D. Pospiech, H. Komber, R. Boldt, A. Lederer, M. El Fray, T. Standau, H. Ruckdäschel, V. Altstädt, B. Voit, *Macromol. Mater. Eng.* **2022**, https://doi.org/10.1002/mame.202200208
[36] C. Okolieocha, D. Raps, K. Subramaniam, V. Altstädt, *Eur. Polym. J.* **2015**, *73*, 500.
[37] B. A. Rodeheaver, J. S. Colton, *Polym. Eng. Sci.* **2004**, *41*, 380.
[38] B. Li, G. Zhao, G. Wang, L. Zhang, J. Gong, *Polym. Degrad. Stab.* **2018**, *156*, 75.
[39] S. Pilla, S. G. Kim, G. K. Auer, S. Gong, C. B. Park, *Polym. Eng. Sci.* **2009**, *49*, 1653.
[40] M. Nofar, Y. Guo, C. B. Park, *Ind. Eng. Chem. Res.* **2013**, *52*, 2297.
[41] M. Lutomski, B. Gawdzik, B. Podkościelna, *J. Therm. Anal. Calorim.* **2016**, *125*, 1425.
[42] K. H. Illers, *Colloid Polym. Sci.* **1980**, *258*, 117.
[43] Y. P. Khanna, W. P. Kuhn, *J. Polym. Sci., Part B: Polym. Phys.* **1997**, *35*, 2219.

